



Impact of tephra falls on Andean communities: The influences of eruption size and weather conditions during the 1999–2001 activity of Tungurahua volcano, Ecuador

Jean-Luc Le Pennec^{a,b,c,*}, Gorki A. Ruiz^d, Patricio Ramón^d, Enrique Palacios^e,
Patricia Mothes^d, Hugo Yepes^d

^a Clermont Université, Université Blaise Pascal, Laboratoire Magmas et Volcans, BP 10448, F-63000 Clermont-Ferrand, France

^b CNRS, UMR 6524, Laboratoire Magmas et Volcans, 5 rue Kessler, 63038 Clermont-Ferrand cedex, France

^c IRD, R 163, Laboratoire Magmas et Volcans, 5 rue Kessler, 63038 Clermont-Ferrand cedex, France

^d Instituto Geofísico, Escuela Politécnica Nacional (IG-EPN), Ap. 17-01-2759, Quito, Ecuador

^e Instituto Nacional de Meteorología e Hidrología (INAMHI), Secretaría Nacional de Gestión de Riesgos, Iñaquito N36-14 y Corea, Quito, Ecuador

ARTICLE INFO

Article history:

Received 31 January 2011

Accepted 26 June 2011

Available online 6 July 2011

Keywords:

Ash fall

Tephra volume

Weather conditions

Andean communities

Tungurahua volcano

Ecuador

ABSTRACT

Repeated ash fall events have occurred during the 1999–ongoing eruption of Tungurahua volcano, Ecuador, notably during the late 1999 and August 2001 eruptive phases. While the eruptive styles were similar, these two phases had different impacts on nearby rural and urban Andean populations: ash falls in late 1999 had limited effects on human health and farming, whereas the 2001 phase resulted in medical problems, death of animals in livestock, and damages to houses and crops. Here we investigate the origin of this difference by estimating the size of the August 2001 event (VEI, magnitude, intensity), and by comparing monitoring information of the 1999 and 2001 phases (duration, explosion rate, column height, SO₂ output rate). The results show that both phases ranked at VEI 3, although the longer 1999 phase was likely larger than the 2001 phase. Mass magnitude (M) and intensity (I) indexes calculated for the 2001 phase reach $M \approx 2.7$ and $I \approx 6.5$ when based on ash fall layer data, but increase to $M \approx 3.2$ and $I \approx 7.0$ when ballistic products are included. We investigated the influence of rain fall and wind flow regimes on ash dispersion, sedimentation and remobilization. The analysis indicates that the harmful effect of the 2001 phase resulted from unfavorable conditions that combined volcanological and seasonal origins, including: a) a low elevation of the ash plume above rural regions owed to a usually bent-over column, b) ash sedimentation in a narrow area west of the volcano under sub-steady wind directions, c) anticipated ash settling by frequent rain flushing of low intensity, and d) formation of a wet cohesive ash coating on buildings and harvests. Conversely, the stronger 1999 phase injected a large amount of ash at higher elevation in the dry season; the ash was widely disseminated across the whole Ecuadorian territory and beyond, and was frequently removed by rain and winds. In summary, our study illustrates the influences of eruption size and weather conditions on the impact of volcanic activity in a tropical setting and puts emphasis on the necessity to merge volcanological and meteorological monitoring duties for hazard assessment and alert level definition, in order to mitigate the effect of ash falls in the Andes and elsewhere.

© 2011 Elsevier B.V. All rights reserved.

1. Introduction

Most explosive andesitic eruptions produce substantial amounts of ash which may impact air traffic, as illustrated by recent eruptions in Iceland and Chile. It may also have significant effect on health, infrastructure and economy at local to multi-provincial scales. Understanding the wide range of hazards associated to transport and deposition of volcanic ash is thus an important issue that has received increasing attention from the international scientific community in the past two decades (e.g. Cronin et al., 1998; Connor et al.,

2001; Casadevall, 2003; Horwell and Baxter, 2006; Stewart et al., 2006; Beddington et al., 2008; Prata, 2009).

Volcanic cloud dispersal and ash fall events have repeatedly taken place near Tungurahua volcano, Ecuador, during the long-lived 1999–ongoing eruptive episode. The eruption has consisted of successive eruptive phases of uneven size and intensity, alternating with periods of relative to complete quietness. As these phases had different impact on nearby Andean communities, we newly introduce here a distinction between *Large* (L), *Moderate* (M) and *Small* (S) *type* phases as useful proxies to describe the size of the events in the context of the 1999–ongoing episode. The most violent L -*type* phases occurred in July and August 2006, February 2008, and May and December 2010, lasted several hours or days, and comprised pyroclastic flow-forming activity and tall eruptive columns (5–13 km above the crater,

* Corresponding author at: IRD, R 163, Laboratoire Magmas et Volcans, 5 rue Kessler, 63038 Clermont-Ferrand cedex, France.

E-mail address: jeanluc.lepennec@ird.fr (J.-L. Le Pennec).

itself located 5 km above sea level, asl) accompanied by scoria and ash falls. The activity was dominated by violent Strombolian to Vulcanian eruptive styles and scoria flow emplacement. These events implied hurried evacuations and resulted in 2006 in six fatalities and severe damages to buildings and farming (BGVN, 1999–2010; Kelfoun et al., 2009; Samaniego et al., 2011). The *M*-type phases typically lasted several days to weeks (e.g. in late 1999, August 2001, October 2003, June 2004 etc.), and consisted of intense degassing with Strombolian to violent Strombolian explosions, lava jets and fountains, and sustained ash emissions, with eruptive columns rising 2–8 km above the crater, but without generation of any pyroclastic flows. However, some *M*-type events had severe impact on economic activities, notably on agriculture and tourism, and occasionally required rerouting of air traffic in central Ecuador. Many other small *S*-type phases had limited or no impact on human activities, when explosions and ash emissions (column height lower than 2.5–3 km above the vent) were too small to affect the populated and cultivated areas.

While the societal outcomes of the 1999–2001 activity has received ample attention (e.g. Lane et al., 2003; Tobin and Whiteford, 2002, 2004; BGVN, 1999–2010; 1999, 2000 and 2001 issues), the volcanology of these distinct eruptive phases has remained poorly known. The size of some *L*-type phases has been estimated and discussed in the

literature (e.g. Eychenne et al., 2012), but the characteristics of *M*- and *S*-type events are still insufficiently documented. However, establishing the eruptive conditions by determining the magnitude, intensity and style of these events, and examining the influence of non-volcanic factors such as weather conditions are important issues to address for understanding the cause of ash impact on rural and urban communities in the Andes in the context of hazard assessment, volcano monitoring, and alert level definition. Here we present the results of such investigation by determining the magnitude and the intensity of the August 2001 phase from ground-based information, and by comparing monitoring data of the 2001 phase with those obtained during the 1999 phase. In addition, we appraise the influence of rain fall and wind flow regimes to gain insights into the cause of the particularly severe impact of the August 2001 eruption.

2. Tungurahua volcano and the 1999–2001 eruptive phases

Tungurahua volcano is located in the southern area of the eastern volcanic row of Ecuador (Hall et al., 2008; Fig. 1). The steep-sided, cone-shaped edifice rises 3 km above the metamorphic basement of the Eastern cordillera, which defines north–south topographic ridges peaking at elevations of ~3.5 km asl. The volcano experienced a major

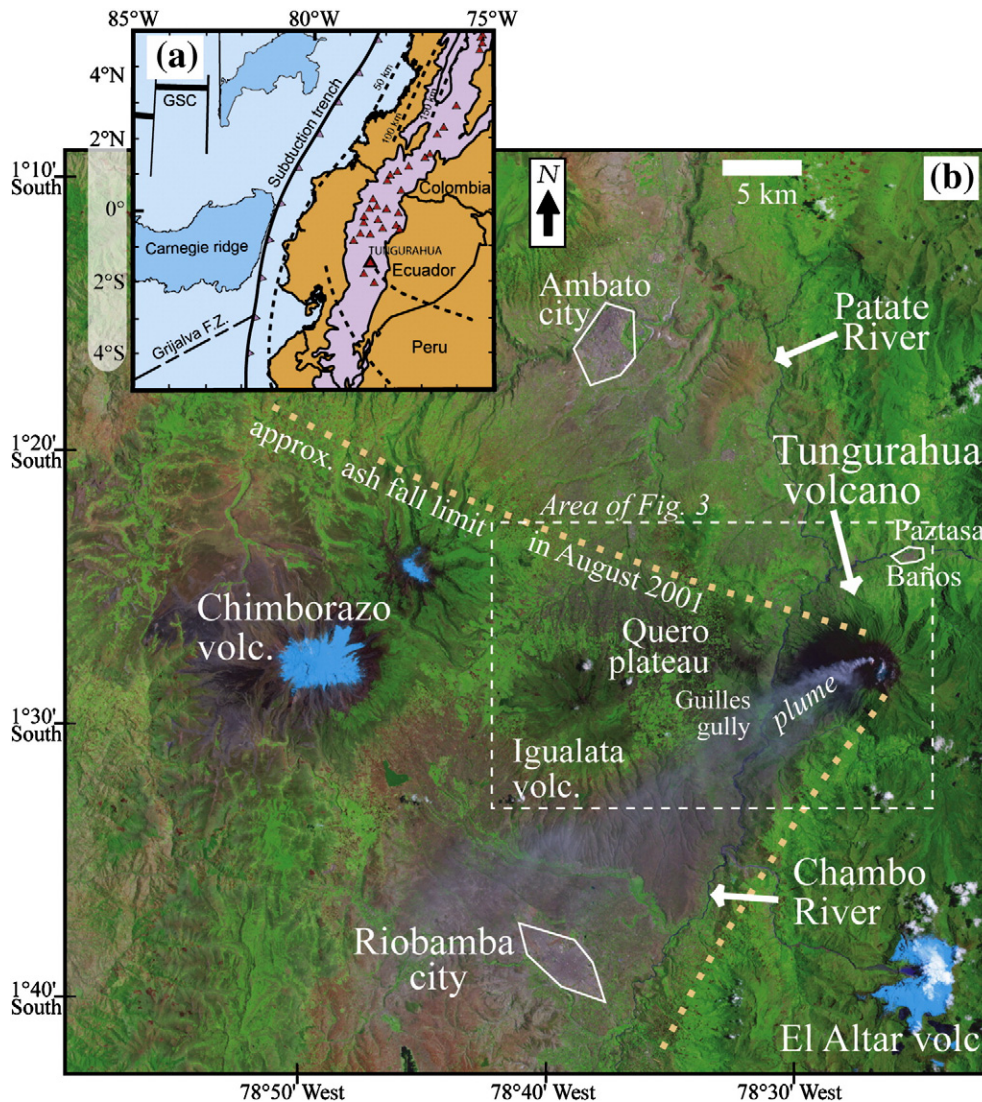


Fig. 1. (a) Location map of Tungurahua volcano in the Ecuadorian volcanic arc. Triangles are quaternary volcanic centers, dashed lines indicate the depth of the Benioff plan, GSC is the Galapagos Spreading center, and G.F.Z. is the Grijalva Fault Zone. (b) Landsat 7's Enhanced Thematic Mapper Plus (ETM+) sensor image of the Tungurahua area during the 2001 eruption. Place names cited in the text are indicated. The dashed box is the study area shown in Fig. 3.

flank collapse at 3 ka BP with a blast event and a debris avalanche, and the new, presently active stratocone witnessed many eruptions of mainly andesitic to dacitic compositions (Hall et al., 1999; Molina et al., 2005; Le Pennec et al., 2006; Samaniego et al., 2011). Pyroclastic flow-forming activity has occurred regularly in the past millennium, with one event per century on average, and historical events took place in 1640, 1773, 1886 and 1916–18 (Almeida and Ramón, 1991; Hall et al., 1999; Le Pennec et al., 2008).

2.1. The late 1999 eruptive phase

After eight decades of quiescence, the volcano progressively reawakened between August and October 1999. After a phreatic vent-clearing onset the magmatic activity began in mid-October (incandescence observed on Oct. 11), followed by alternating phases of gas and ash emissions, and Strombolian to violent Strombolian eruptive styles. Many canon-like shots associated to short-lived “vulcanian-like” and violent Strombolian explosions were seismically recorded from Oct. 28 onward (Ruiz et al., 2005), sending eruptive columns higher than 3 km above the crater, and occasionally up to ~7 km (12 km asl). The activity declined at the end of the first week of December 1999, when column height decreased below ~7.6 km asl on average, with lower ash content in the plume. This first eruptive phase (October 28 to December 10) lasted 6 weeks, thus totalizing 42 days of intense activity, and is hereafter called the “late 1999” phase. At Tungurahua, in the context of the 1999-ongoing eruptive episode, the above column height threshold at 7.6 km asl (i.e. ~2.5–3 km above the crater, depending on wind velocity) typically discriminates the eruptive columns of *S-type* events (low frequency of explosions, column height usually below ~7.6 km asl, rare incandescent blocks and bombs outside of the crater, little acoustic activity) with those of *M-* and *L-type* events (high frequency of explosions, column height frequently above ~2.5–3 km, large amounts of incandescent blocks and bombs expelled outside of the

crater, intense acoustic activity with explosions heard at distances exceeding 20–30 km). This late 1999 phase prompted the evacuation of >20000 people threatened by pyroclastic flows near the volcano.

2.2. The August 2001 phase

The intensity of the eruption increased again in late December 1999 and fluctuated during year 2000, and then decreased drastically in October of the same year. After seven months of quiescence, a new eruptive phase preceded by deep LP seismic events started in late May 2001 with small-scale lava fountains, accompanied by explosions in June and July (Le Pennec et al., 2002, 2004). With no clear precursory warning, a strong increase in tremor amplitude took place on August 4, 2001, marking the onset of a new intense eruptive phase. When observable, the eruption consisted of Strombolian to violent Strombolian styles (explosions with copious ballistic ejections, lava jets and ash emissions), and the acoustic activity comprised canon-like shots and frequent rumbling noises. This activity gave rise to a sustained, commonly bent-over column, typically 2–4 km-high above crater level, which usually drifted west (SW to NW, Fig. 2a) and mixed with meteorological clouds. The phase clearly commenced on August 4, but the eruptive intensity declined irregularly during several days after the powerful August 16 lava fountaining event. We consider that the deposition of ash in the studied area ended on 20–21 August, when the column height declined to less than ~2 km above the crater. On August 23, a modest gas plume with very low ash content was observed above the crater. This yields duration of 17–18 days (2.5 weeks) for this intense eruptive activity, which is referred below to as the “August 2001” phase.

2.3. Deposits and impacts of the 1999–2001 activity

The thin deposits of the late 1999 activity were frequently removed by erosion, but field studies on the western flanks of Tungurahua

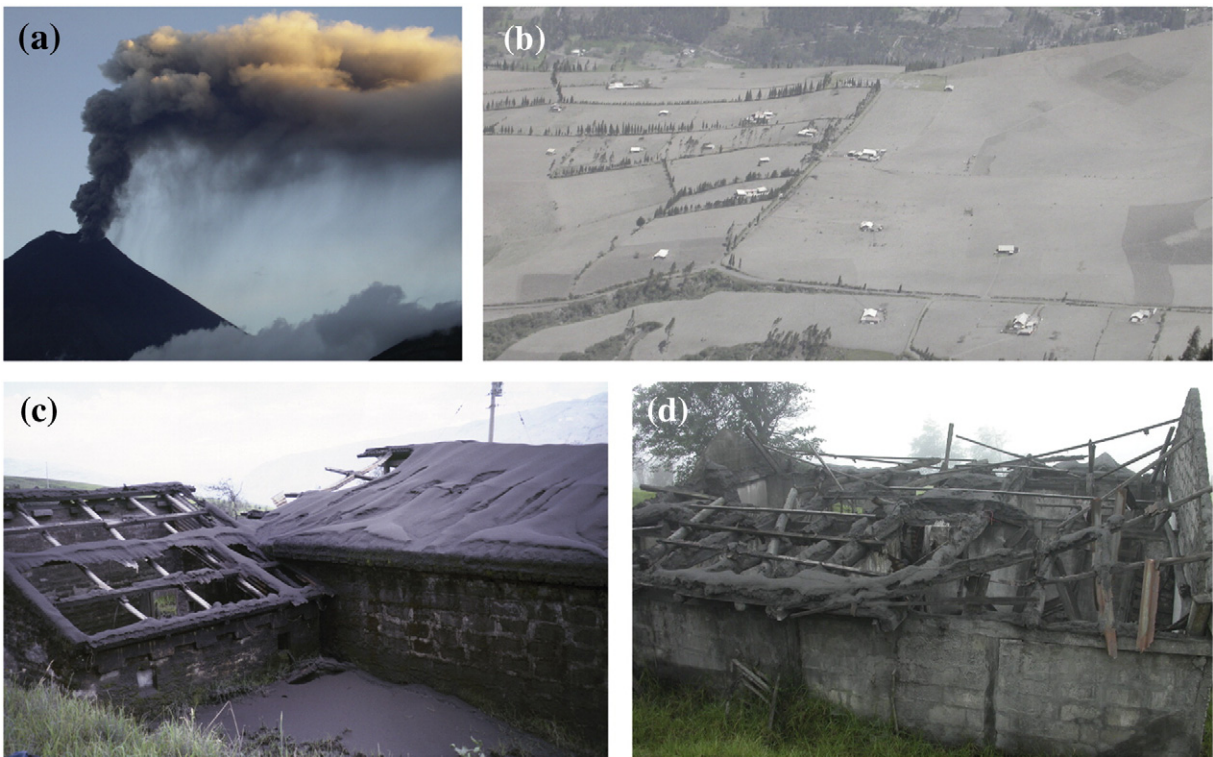


Fig. 2. Photos of Tungurahua ash falls and their impacts during *M-type* eruptive phases, in the course of the present eruptive episode (1999-ongoing). (a) A typical ~2.5–3 km high, slightly bent-over column in Oct. 2003. Note the dark ash fall curtain below the plume and meteorological clouds at about 3–3.5 km asl. (b) Cultivated lands covered by ash deposited during the Oct. 2003 eruptive phase. (c) Ash accumulated on roofs on the western flank at the end of the August 2001 eruption. Damage to the zinc roof on the left is essentially due to corrosion by acid rains, and not only to the weight of ash (ash thickness at that place was ~7 cm). (d) Collapsed roof after the Nov. 2004 eruptive phase.

indicated that the tephra comprised a lower reddish fine-grained layer corresponding to phreatic outbursts of Sept.–Oct. 1999, overlain by a grayish bed of moderately vesiculated andesitic ash. Ash falls and wind remobilization caused health problems, with some respiratory and skin/eye diseases (OPS, 2000; Lane et al., 2003) and troubles to livestock and crops, but in general the impact was rather limited and confined to proximal areas (<8 km from the crater). The deposit of the August 2001 eruption consisted of a continuous, dark-toned coating of wet ash on the flanks of the edifice and on the rural Quero plateau located ~8–30 km down prevailing winds from the volcano (Figs. 1b and 2b). In most localities the tephra bed occurred as a laminated, well sorted layer composed of andesitic ash particles, whose composition (~58 wt.% SiO₂) is close to that of other eruptive phases of the 1999-ongoing episode (Samaniego et al., 2011). Highly vesiculated clasts typically made ~30–50% of the grain population, while moderately vesiculated particles accounted for about 20%. Noticeably, non-vesiculated juvenile grains represented about 30–40% of the particles in the layer. The deposits also contained reddish xenoclastic elements (about 3–4%), and free crystals whose proportion varied from 0 to about 12% depending on grain size and locality.

The impact of the 2001 phase was severe and prompted the intervention of several national and international humanitarian organizations (BCVN, 1999–2010, 2001 issue). According to a report of the United Nations Office for the Coordination of Humanitarian Affairs released on Sept. 5, 2001 it is estimated that near 40000 people had been affected by the volcano, resulting in heightened respiratory infections. In addition, more than 3000 houses were damaged (Fig. 2c and d) and potable water supplies were contaminated by volcanic ash, thus requiring water-quality monitoring. Wet ash falls and associated acidic rains affected livestock and agricultural resources over an area of >50000 ha to the west of the volcano (Fig. 2b), forcing local evacuations of cattle, which suffered death of animals by ingestion of contaminated grass and leaves. Hence, the August 2001 event of Tungurahua was the first eruptive phase that had a pronounced impact on nearby Andean communities, twenty-three months after the onset of the magmatic activity in October 1999.

3. Data collection

3.1. Monitoring data

The 1999-ongoing eruptive episode has been closely monitored by the Instituto Geofísico–Escuela Politécnica Nacional (IG–EPN in Quito, Ecuador). Surveillance techniques include eyewitness observation of the activity (weather permitting) from the observatory and elsewhere, seismic recording from 5 to 10 stations, frequent SO₂ monitoring, and DEM-tiltmeter surveying. SO₂ flux estimation during the 1999–2001 phases was carried out with a Cospec instrument, using traverse and static measurement protocols (Arellano et al., 2008). In addition, freely available NOAA–VAAC satellite images (<http://www.ssd.noaa/VAAC/ARCHIVE/gifs/tung>) were inspected to assess eruptive column elevations and plume dispersal patterns in Ecuador and beyond. We calculated mean ash cloud elevations and delineated their limits on all relevant satellite images collected in the time intervals Oct.–Dec. 1999 and June–Sept. 2001 (Ruiz et al., 2004). To account for the qualitative eruptive intensity threshold given earlier (i.e. column height below or above ~7.6 km asl), we outlined all plumes identified at low elevation (<7.6 km asl.) from those detected at higher altitude. Obviously these images are to be used with caution, but they offer a useful proxy to describe the eruptive phases on a multi-weeks scale.

3.2. Thickness data and isopach map reconstruction

Prohibited access to the volcano in late 1999, tephra thickness values in accessible areas near or below the measurable limit (thickness $T < 1$ –2 mm), and frequent ash removal by winds and rain waters hampered

obtaining a reliable isopach map for the late 1999 eruptive phase. Conversely, the wet, cohesive nature of the ash deposited in August 2001 offered favorable conditions to obtain reliable thickness measurements within several weeks of the emplacement of the ash layer before erosion. Several measurements were collected at 91 sites to obtain averaged rain-compacted thickness values, and a plot of distance from source (d) vs. thickness (T) reveals the segmented pattern of the deposit, with a prominent inflexion at ~6 km (Fig. 3a). We contoured twelve isopachs in the thickness range of 0.3–12 cm on a map (Fig. 3b) and assessed the area (A) of two distal isopachs based upon the following arguments. On the Pan-American Highway a thickness of 0.2 cm of ash was measured 28 km downwind from the volcano. Considering an elliptical isopach 28 km long and 14 km wide (i.e. isopach aspect ratio of 2, slightly smaller than that of the medial deposits) we obtain an area of 308 km². In addition, the icecap of Chimborazo volcano, located about 50 km west of Tungurahua (Fig. 1), appeared coated with a dark layer of ash at the end of the eruption. By analogy with what we have observed at many other localities near Tungurahua, we inferred that a minimum thickness of 0.05 cm is required to obtain such a uniform ash cover. This led us to define the area of the 0.05 cm isopach as that of an ellipse 50 km-long and 20 km-wide. We also bounded the area of little or no ash fall deposition in proximal–medial areas (noted “traces” in Fig. 3c). To define on a gross scale the distal depositional limit (i.e. to infer the area of the isopach $T=0$), we inspected ash clouds in NOAA satellite images, and along with eyewitness accounts of light ash fall near the Ecuadorian coast between Manta and Guayaquil cities, we set the westernmost limit of the $T=0$ isopach in coincidence with the 81° meridian, off the Ecuadorian coast (Fig. 1). We thus approximate the $T=0$ isopach area to that of a 300 × 80 km ellipse, i.e. 18,850 km². Data of isopach thicknesses and areas are given in Table 1.

3.3. Ballistic material data

The 2001 activity also consisted of many explosions and lava fountains, which showered the summit area with incandescent bombs and blocks. The access to the crater has remained extremely dangerous for months, making field work difficult to estimate the amount of ballistic products. Nevertheless, observations from Tungurahua Volcano Observatory and elsewhere at the end of the eruption indicated that the small glacier on the northern crater edge was covered by a dark layer whose thickness was about twice the height of the mountain refuge located at 3800 m asl on the northern flank of the volcano. We thus roughly estimated the thickness of the ballistic layer at that place at $h \approx 10$ –20 m. Direct observation and inspection of night-time photos/videos and topographic maps indicate that most ballistic clasts impacted the ground within a circle of radius $R \approx 600 \pm 100$ m around the active vents, before descending the slopes for hundreds of meters in remote gullies. The density of the ballistic tephra deposit was also difficult to evaluate because of access problems, but observations and sampling during and after the 1999–2001 eruptive phases revealed that most ballistic clasts consisted of poorly vesiculated sub-vitric blocks and bombs.

3.4. Weather data

Tungurahua volcano sits in the meteorological “Intertropical Convergence Zone” where humid, westward-moving air masses above the Amazonian lowlands condensate against the Eastern Cordillera of Ecuador, notably on the Eastern flank of the edifice. Because of high reliefs, sharp topographic irregularities and strong temperature–moisture gradients in the area, the Tungurahua region is a patchwork of many microclimates. This pattern is further complicated by diurnal–nocturnal and seasonal instabilities, which all make representative climate characterization difficult to obtain at this tropical volcano, and current weather networks do not document adequately this variability.

Rain fall data were not collected at Baños weather station (1800 m asl) in late 1999 during the evacuation period. To obtain a reliable

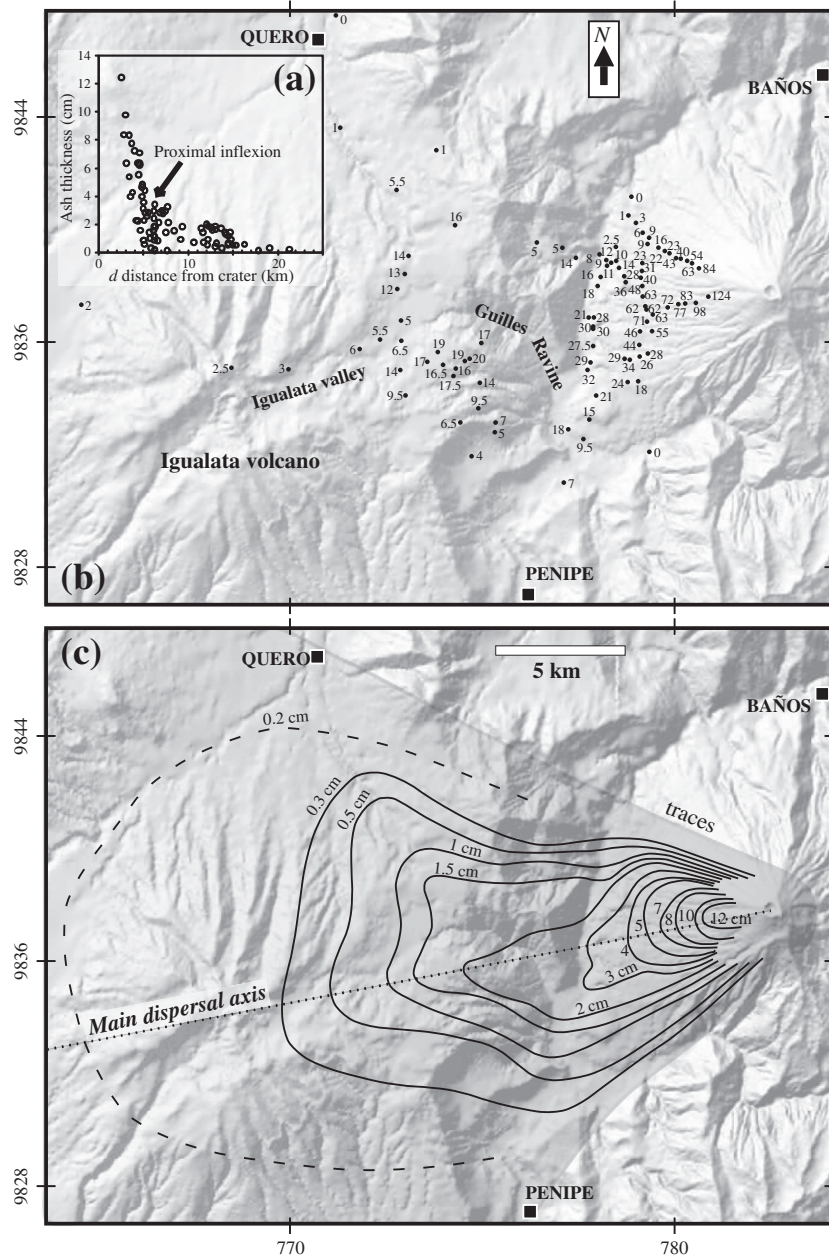


Fig. 3. Thickness data and isopach reconstruction for the 2001 tephra fall deposit. (a) Plot of ash thickness vs. distance from the crater for all sites. (b) Map of the area west of Tungurahua volcano showing thickness data (in mm) and (c) resulting isopach contours (in cm). The main dispersal axis in the Tungurahua region and beyond is indicated with a dashed line. UTM coordinates refer to the South America 145 prov. S.A. 1956, Ecuador Zone 17 N (84°W–78°W).

proxy and to describe the precipitation regime in a similar period of the year in Baños, we collected rain fall data for November and December in the period 1983–2008 from INAMHI archives in Quito headquarter and selected all complete files to obtain 17 and 16 years of record for November and December, respectively. As both months have similar climate regimes, they are treated together below. Wind flow is documented here using forecasted wind directions and velocities calculated by NOAA–GDAS models (Ruiz et al., 2004).

4. Methods

4.1. Tephra volume calculations

The method for estimating the ash fall layer volume differs from that used for the ballistic material; here we first present ash fall volume calculations before considering the case of the ballistic

tephras. Previous studies have shown that the volume of many ash and lapilli fall deposits can be obtained by assuming exponential or power law decay rates, which enable *parametric* bulk volume estimation (Pyle, 1989; Fierstein and Nathenson, 1992; Pyle, 1995; Bonadonna et al., 1998; Legros, 2000; Bonadonna and Houghton, 2005; Sulpizio, 2005). However, because tephra fall deposits do not necessarily follow a simple thinning pattern, we combine here different methods to infer the most reliable (rain-compacted) bulk ash fall layer volume. First, the volume may be determined without making any assumption on the “theoretical/parametric” decay rate, by simply relying on the geometry of the deposit, as described by data on tephra thickness and isopach areas. Minimum and maximum volumes may thus be estimated from simple geometric elements that bracket the decay rate (Fig. 4). A maximum volume is obtainable with the “trapezoidal rule” approximation of Froggatt (1982) and Fierstein and Nathenson (1992) and a minimum volume can be estimated using a

Table 1

Characteristics of the August 2001 tephra fall deposit from Tungurahua with thickness and areal data of the isopachs contoured in Fig. 3c. The uncertainty on thickness is an estimate based on repeated measurements (typically 3 to 8 thickness determinations) at most localities. The 0.05 cm isopach is roughly estimated from the observed ash cover on Chimborazo icecap, and the uncertainty is not determinable (n.d.).

Isopach thickness (in cm)	Estimated uncertainty on thickness (in cm)	A (in km ²)
12.0	0.4	2.02
10.0	0.4	3.82
8.0	0.3	6.74
7.0	0.3	9.10
5.0	0.2	12.52
4.0	0.2	14.98
3.0	0.2	20.12
2.0	0.2	37.31
1.5	0.1	60.00
1.0	0.1	80.68
0.5	0.05	116.36
0.3	0.05	165.27
0.2	0.05	307.88
0.05	n.d.	785.40

simple “nested rings” approximation (Le Pennec et al., 2002, see below). Both *non-parametric* methods entail a large number of isopach in the analysis, a requirement that is reasonably met in the present study for the August 2001 phase with >12 isopach contours (Fig. 3b). Secondly, *parametric* volume calculations can be made using selected models and input data. Here, we calculated the tephra fall volume using different expressions of the literature, by incorporating one or two segments with dissimilar decay rates and inflexion points (IP).

4.1.1. Non-parametric methods

The “trapezoidal rule” overestimates the true volume (see details in Fierstein and Nathenson, 1992), but tends to give acceptable maximum values when closely spaced isopachs are provided and when a $T=0$ isopach can be defined. It also requires estimating T_0 , the ash fall thickness at the vent. According to a mountain climber who reached the crater in December 2001, the fallout thickness on the northern upper slopes was about 40–60 cm (Alexander García, pers. comm., 2001). Because the dispersal axis was oriented to the west of the crater, and since the crater margin is still situated about 100–125 m from the major eruptive vents, we have assigned in this case a minimum value of 80 cm for T_0 (i.e. excluding the ballistic material considered below). The method considers that the thinning rate is a discontinuous function of isopach area and thickness varies linearly with A between two successive isopach data (Fig. 4).

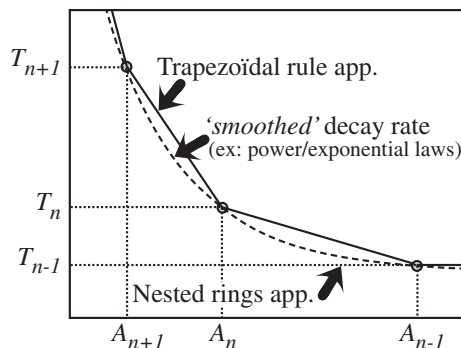


Fig. 4. Plot of thickness vs. area, showing the principle of non-parametric ash volume estimates, including *trapezoidal rule* (solid line) and *nested rings* (dotted line) approximation methods. The interpolated “smoothed” thinning law is shown as a dashed curve.

The “nested rings approximation” (Le Pennec et al., 2002) consists in dividing the ash fall layer in a succession of concentric structures (or eccentric for elliptical isopach contour shapes), each being bounded by two isopachs of thickness T_n and T_{n-1} (with $T_n > T_{n-1}$), corresponding to areas A_n and A_{n-1} ($A_{n-1} > A_n$) respectively (Fig. 4). Between T_n and T_{n-1} the thickness is set as constant and equal to T_{n-1} . Because thinning rates are markedly concave down in T vs. A or $A^{1/2}$ plots, the approximation by this method may approach reasonably the interpolated decay rate. This method necessitates no extrapolation to the vent or to infinity but requires many closely spaced isopachs to provide a reliable minimum volume.

4.1.2. Parametric methods

The interpolation by a single exponential thinning law of the form $T = T_0 \exp(-k \times A^{1/2})$ allows calculating a volume V using the equation (Pyle, 1989): $V = 13.083 \times T_0 \times b_t^2$, where T_0 is the extrapolated thickness at the vent ($d=0$), k is the coefficient of the exponential decay, and b_t is the thickness half distance defined by $b_t = \ln(2)/(k \times \pi^{1/2})$. Previous works since Pyle (1989) and Fierstein and Nathenson (1992) have shown that the data for many natural deposits plot as one or two straight lines on a $\log T - A^{1/2}$ diagram. From these and other findings, it has been inferred that the thickness of most proximal and medial tephra fallout deposits thin exponentially with distance from the source, and many models of tephra fall volume calculations are based on this assumption (e.g. Pyle, 1989, 1995; Fierstein and Nathenson, 1992; Houghton et al., 2000; Legros, 2000; Sulpizio, 2005). However, Bonadonna et al. (1998) investigated the influence of particle Reynolds numbers on final tephra fall thickness and found that the settling of fine-grained ash with low Reynolds numbers should form a deposit whose thinning rate is better described by a power law of the form: $T = T_{pi} A^{-m/2}$, where T_{pi} is a constant and m is the power-law coefficient. The volume V is then given by: $V = (2 T_{pi} / (2 - m)) \times (C^{2-m} - B^{2-m})$, where B and C are the integration limits in proximal and distal areas, respectively (Bonadonna and Houghton, 2005). B can be set as the distance of the calculated maximum thickness (T_0), and is obtained with: $B = (T_0 / T_{pi})^{-1/m}$. This expression yields 1.37 km for the 2001 phase and thus the volume estimates neglect the proximal deposit. Hence, we also calculated with $B = 1$ km (i.e. beyond the area of ballistic impacts). We set the distal limit ($A^{1/2}$) to 60 km, nearly corresponding to the 0.05 cm isopach area, and to 140 km, approximately coinciding with the $T=0$ isopach area defined for the trapezoidal rule method. We also calculated the volume using a two-segmented decay rate with power law interpolations on $\log T - \log A$ plots, using Rose et al. (1973) expression: $V = A_{ip} T_{ip} \times [(1/(c_1 + 1)) - (1/(c_2 + 1))]$, where A_{ip} and T_{ip} are isopach area and thickness at the inflexion point (subscript “IP”) on the log-log plot, and c_1 and c_2 are the decay coefficients for the power laws of the distal and proximal segments, respectively.

Volume estimates based on $\log T$ vs. $A^{1/2}$ plots using two exponential segments with different limits and inflexion points were calculated using the expression of Fierstein and Nathenson (1992), with: $V = (2 T_0 / k^2) + 2 T_0 \times [((k_1 A_{ip}^{1/2} + 1) / k_1^2) - ((k A_{ip}^{1/2} + 1) / k^2)] \times \exp(-k A_{ip}^{1/2})$, where k and k_1 are the decay parameters of the proximal and distal segments, respectively. We also calculated the minimum tephra volume using $V = 3.69 \times T \times A$, from the single isopach approach of Legros (2000), which is based on the exponential thinning rate hypothesis.

Distal ash falls and their impact on volume estimation have remained a major challenge in tephra studies; empirical equations have been proposed for large scale explosive eruptions (Sulpizio, 2005), but the applicability to eruptions of smaller size with weak volcanic column, as that of Tungurahua in 2001, is still untested. Assuming the exponential decay rate, Pyle (1995) proposed to incorporate distal deposits in tephra volume calculations using the expression: $V_{pm} / V_{total} = 1 - (T_{last} / T_0) (1 - \ln(T_{last} / T_0))$, in which V_{pm} is the volume of proximal and medial deposits (subscript pm).

To convert these volumes in masses we determined in the laboratory the density of five mechanically compacted dry ash samples, an obtained $1.0 \pm 0.1 \text{ g/cm}^3$. This value is considered as representative of the whole layer and is similar to that reported for proximal–medial deposits after the August 2006 Tungurahua paroxysm (Eychenne et al., 2012), and at other volcanoes, e.g. Mt St Helens (Sarna-Wojcicki et al., 1981) Rebutot (Scott and McGimsey, 1994), Mout Spurr (McGimsey et al., 2002), all three in the USA, and at Ruapehue in New Zealand (Bonadonna and Houghton, 2005).

4.1.3. Volume and mass of ballistics

We assume that the amount of ballistic products can be described as that of a low cone, whose volume V is given by $V = [1/3 \times (\pi \times h) \times (R^2 + r^2 + R \times r)] - (\pi \times r^2 \times h)$, where r is the crater radius, set at 100–125 m. The second term in the expression aims at discarding the unpreserved intra-crater products, depicted as a low cylinder of radius r and height h . For mass conversion we assume a density of 2.65 g/cm^3 for a pore-free andesite with 58% SiO_2 (Samaniego et al., 2011), and a bulk deposit porosity of 30%, in which 20% and 10% account for inter- and intra-particle porosities, respectively.

4.2. Inferring the size of the eruptive phases

Our ground-based data for the 2001 phase allow us to infer the Volcanic Explosivity Index (VEI) of Newhall and Self (1982). To address the discretization concern faced in the VEI scale we convert to mass to calculate the indexes of Pyle (2000) with magnitude: $M = \log_{10}$ (erupted mass, in kg) – 7; intensity: $I = \log_{10}$ (erupted mass per unit time, in kg/s) + 3. The late 1999 phase was not adequately characterized with ground-based data; we thus infer its size by comparing a posteriori the late 1999 monitoring data (duration, seismic activity, column heights, SO_2 output rate), with those of the 2001 phase. For this reason, our results are first presented below for the August 2001 phase, before considering the late 1999 phase.

4.3. Meteorological analyses

To compare the meteorological regime during both phases we first calculate the total and daily rain fall height for the 2001 phase. As rainfall data were unavailable at Baños weather station in late 1999, we calculate the monthly and daily average for selected years in the 1983–2008 interval and compare with the pattern observed at other weather stations in central Ecuador in Nov.–Dec. 1999. Forecasted wind direction data compiled for time intervals of both eruptive phases are grouped at 20° intervals and ash plumes distribution in Ecuador and beyond is examined from NOAA–VAAC images. We then appraise the influence of short-term (daily) and mid-term (seasonal) influences on tephra dispersal behavior.

5. Results

5.1. The August 2001 phase

5.1.1. Monitoring results

The seismic network at IG–EPN recorded 132 explosions in the 4–21 August 2001 time interval, i.e. an average of 7.5 explosions/day, along with sub-continuous tremor and ash emission signals. All reliable Cospec measurements yielded SO_2 output rates below 4 kt/day (Ruiz et al., 2004; Arellano et al., 2008). The 72 satellite images reveal that 72% of the ash clouds were detected above 7.6 km asl, and 28% below, with an average elevation at 8.4 km asl during the 4–21 August 2001 period.

5.1.2. Tephra thinning rate, volume and mass

The isopach map (Fig. 3b) shows a main dispersal axis to the W–SW of the crater, and bilobate contour shapes are noted near

Igualata volcano. Isopach aspect ratio (long/short axes ratio) of about 2.2 ± 0.5 suggests moderate wind speeds at plume elevation, consistent with mean velocities of $\sim 10 \text{ m/s}$ forecasted by NOAA–GDAS models. Fig. 5a compares T vs. distance from the vent (d) for selected sites located close to the main dispersal axis (Fig. 3b). Both exponential and power laws fit the data well, i.e. with $R^2 > 0.94$. The power law has a slightly lower fit but only two data occur out of the regression curve, at ~ 12 – 13 km from the crater, a distance which coincides with isopach irregularities near the deep Guilles Ravine (Figs. 1 and 3a). A plot of T vs. $A^{1/2}$ (Fig. 5b) exhibits a quite regular decay rate, although uncertainties depicted as grayed boxes may hide complications. The pattern displayed on a graph $\log T$ vs. $A^{1/2}$ (Fig. 5c) departs from the classical single- or bi-segmented form of many tephra decay rates and the small concave-up “bulge” observed in the thickness range of ~ 2 – 0.5 cm may be described as a “secondary thickening” area.

Our volume calculation results are given in Table 2 for a selection of 24 runs, using non-parametric and parametric approaches (Le Pennec et al., 2002, 2004). Calculations made with the trapezoidal rule approximation (runs 1 to 4 in Table 2) yield a bulk cumulative volume V_{tr} (subscript “tr” is for “trapezoidal rule”) of $3.21 \times 10^6 \text{ m}^3$ when the most distal isopach has a thickness $T_{last} = 0.3 \text{ cm}$; $4.01 \times 10^6 \text{ m}^3$ with $T_{last} = 0.05 \text{ cm}$, and $8.52 \times 10^6 \text{ m}^3$ with $T_{last} = 0$. This latter value is a maximum estimate of the ash layer volume. Application of the nested rings approximation to our data collection (runs 5 to 8) gives a

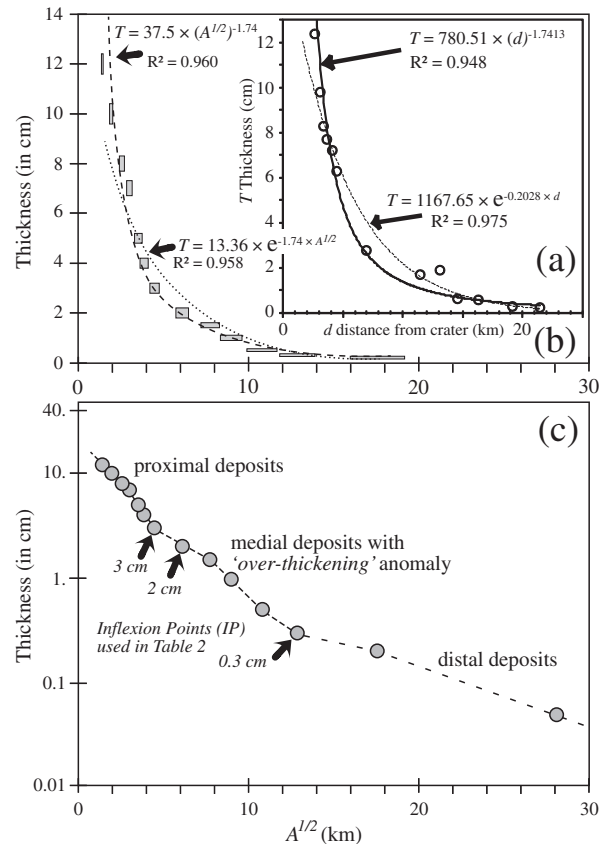


Fig. 5. Decay pattern of the August 2001 tephra layer from Tungurahua volcano. (a) Ash fall thickness vs. distance from the crater for 13 selected sites close to the main dispersal axis, i.e. W–SW of the volcano (shown in Fig. 3c). (b) Plot of T vs. $A^{1/2}$ showing the estimated uncertainties as boxes on both thickness values and isopach areas. We estimated the error on thickness at $\sim 5\%$ on average, with an increase from 4% in proximal areas ($T > 4 \text{ cm}$) to $\sim 8\%$ in median areas ($1 < T < 4 \text{ cm}$) and above 10% in distal areas. We considered a minimum uncertainty of about 7% on each isopach area A . Exponential and power law interpolations are depicted as dotted and dashed curves, respectively. R^2 are coefficients of determination. (c) Plot of $\log T$ vs. $A^{1/2}$, with indication of the inflexion points introduced in tephra volume calculations (Table 2).

Table 2

Models and parameters for calculating bulk tephra fall volume of the August 2001 eruptive phase from Tungurahua and results in millions of cubic meters.

Method (number of segments) (reference)	Parameters and coefficients								Volume (10 ⁶ m ³)		
Trapezoidal rule approx. Froggatt (1982)	T_{last}										
Run 1 (12 segments)	cm										
Run 2 (13 segments)	0.3								3.21		
Run 3 (14 segments)	0.2								3.53		
Run 4 (15 segments)	0.05								4.01		
	0								8.52		
Nested rings approx. Le Pennec et al. (2002)	T_{last}										
Run 5 (5 segments)	cm										
Run 6 (12 segments)	5								0.99		
Run 7 (13 segments)	0.3								2.46		
Run 8 (14 segments)	0.2								2.75		
	0.05								2.98		
Plot $\log T-A^{1/2}$ (1 segment) Bonadonna and Houghton (2005)	T_0	k	R^2	B	C						
Run 9	cm			km	km						
Run 10	24.909	-1.8742	0.9626	1.369	60				4.49		
Run 11	44.686	-1.8742	0.9626	1.000	60				4.78		
Run 12	24.909	-1.8742	0.9626	1.369	140				5.83		
	44.686	-1.8742	0.9626	1.000	140				6.11		
Plot $\log A-\log T$ (2 segments) Rose et al. (1973)	T_{last}	c_1	R_1^2	c_2	R_2^2	T_{ip}	A_{ip}				
Run 13 (IP = 3 cm) (IP = Inflexion Point)	cm					cm	km				
Run 14 (IP = 2 cm)	0.3	-0.857	0.9397	-1.544	0.9159	2.7730	28.050			6.85	
Run 15 (IP = 0.3 cm)	0.05	-0.797	0.9856	-1.463	0.9418	1.9500	43.039			5.94	
	0.05	-0.820	0.9643	-1.133	0.9499	0.79338	84.476			8.75	
Plot $\log T-A^{1/2}$ (1 segment) Pyle (1989)	T_{last}	T_0	b_t	k	R^2						
Run 16	cm	cm	km								
Run 17	1.5	18.3210	1.1167	0.3502	0.9602					2.99	
Run 18	0.3	16.5430	1.2217	0.3201	0.9863					3.23	
	0.05	9.1617	1.8172	0.2152	0.9293					3.96	
Plot $\log T-A^{1/2}$ (2 segments) Fierstein and Nathenson (1992)	T_{last}	T_0	k	R_1^2	T_1	R_2^2	k_1	$A_{ip}^{1/2}$			
Run 19 (IP = 3 cm)	cm	cm			cm			km			
Run 20 (IP = 2 cm)	0.3	24.909	0.4596	0.9808	11.519	0.9878	0.2818	4.48553			3.25
Run 21 (IP = 0.3 cm)	0.05	21.789	0.4094	0.9771	36.729	0.9424	0.1553	6.10819			4.74
	0.05	16.543	0.3201	0.9863	36.729	0.9920	0.1205	12.8557			3.91
Single isopach approx. Legros (2000)	T	A									
Run 22	cm	km ²									
Run 23	2.0	37.31								2.75	
Run 24	1.5	60.00								3.32	
	1.0	80.68								2.98	

The most proximal isopach used in the calculations is set at $T_{first} = 12$ cm for all runs.

T_{last} is the most distal isopach thickness used in the calculations (Pyle, 1995).

T_0 : extrapolated thickness at the vent ($d = 0$).

B and C : power law integration limits in proximal and distal areas, respectively.

k : coefficient of the exponential and power law decay rates.

k_1 : coefficient for the distal segment in the bi-segmented power law decay rate.

b_t : thickness half distance, distance over which the thickness has decreased by half.

A_{ip} : tephra thickness at the selected inflexion point in the decay rate.

T_{ip} : the isopach area at the selected inflexion point in the decay rate.

c_1 and c_2 : decay parameters for power laws of distal and proximal segments, respectively.

R_1^2 and R_2^2 : coefficients of determination (goodness of fit) for proximal and distal segments, respectively.

cumulative volume V_{nr} (subscript "nr" is for "nested rings") of 2.46×10^6 m³ when the most distal isopach T_{last} has a thickness of 0.3 cm, 2.75×10^6 m³ with $T_{last} = 0.2$ cm, and 2.98×10^6 m³ with $T_{last} = 0.05$ cm. This latter value is a minimum estimate of the bulk ash fall layer volume.

Calculations using single power law decay with different integration limits (Bonadonna and Houghton, 2005) yield volumes in the range of 4.49 – 6.11×10^6 m³ (runs 9 to 12). When two power law segments are considered with T as the independent coordinate in a plot $\log A-\log T$ (Rose et al., 1973; runs 13 to 15 in Table 2), the volume varies from 5.94 to 8.75×10^6 m³, depending on the position of the inflexion point (3, 2, and 0.3 cm) and of T_{last} (0.3 and 0.05 cm). We note that run 15 yields a slightly higher volume than run 4 in the trapezoidal rule approach. An exponential thinning rate with a single segment

(Pyle, 1989) and different T_{last} values give a tephra fall volume in the range of 2.99 to 3.96×10^6 m³ (runs 16 to 18). Volume estimates based on $\log T$ vs. $A^{1/2}$ plots (Fig. 5c) using two exponential segments (Fierstein and Nathenson, 1992) with different T_{last} and inflexion points (IP), yield results from 3.25 to 4.74×10^6 m³ (runs 19–21).

These estimates do not include very distal (i.e. >200 km downwind) tephra fall deposits. To evaluate the impact of the distal ash on volume calculations we used the expression of Pyle (1995); for example, discarding the less well defined distal isopachs in run 17 (i.e. one exponential segment with $T_{last} = 0.3$ cm), we obtain $T_{last}/T_0 = 0.018$, and the ratio $V_{pm}/V_{total} = 0.91$, implying $V_{total} = 3.55 \times 10^6$ m³, i.e. ~10% larger than the volume inside the 0.3 cm isopach. We also calculated the minimum tephra volume using the single isopach approach of Legros (2000), and obtained results that are significantly

lower than those of previous models. The highest value at $3.32 \times 10^6 \text{ m}^3$ is obtained for the 1.5 cm isopach (runs 22 to 24).

Altogether, runs 9 to 21 based on parametric decay rates yield fairly consistent results which compare to those obtained with non-parametric approximations. Tephra volumes obtained at $T_{\text{last}} = 0.05 \text{ cm}$ assuming bi-segmented decay rates are between 3.91 and $8.75 \times 10^6 \text{ m}^3$, i.e. with a factor of only 2.24 between these extremes, while non-parametric methods give results between 2.98 and $8.52 \times 10^6 \text{ m}^3$ down to an extrapolated $T = 0$ isopach. Hence, these results reasonably support an ash layer volume on the order of $6.0 \pm 3.0 \times 10^6 \text{ m}^3$, which convert to a total mass of ash of $2.7\text{--}9.9 \times 10^9 \text{ kg}$ for a bulk layer density of $1.0 \pm 0.1 \text{ g/cm}^3$.

Using data and cone geometry assumptions given earlier for the ballistic material, we obtain a bulk volume of $6.6 \pm 2.5 \times 10^6 \text{ m}^3$, i.e. similar to that of the plume-generated ash layer, which convert to a DRE volume of $2\text{--}8 \times 10^6 \text{ m}^3$, and to a mass in the range of $5.4\text{--}21.2 \times 10^9 \text{ kg}$. Summing volumes and masses of ash and ballistic deposits yields a total bulk tephra volume in the range of $5.9\text{--}20.4 \times 10^6 \text{ m}^3$, and a total mass in the range of $8\text{--}30 \times 10^9 \text{ kg}$.

5.1.3. Magnitude and intensity of the August 2001 phase

The above results allow us to constrain the magnitude and the intensity of the eruption, which are useful descriptors of the *M*-type August 2001 phase. The calculated ash fall volume indicates that this phase would rank at VEI 2 (Newhall and Self, 1982), corresponding to moderate explosive eruptions with column heights of 1–5 km above the crater, Strombolian to Vulcanian eruptive styles, and a tephra volume in the range of $1\text{--}10 \times 10^6 \text{ m}^3$. However, incorporating the ballistic deposits in eruption size estimates yields values above

$10 \times 10^6 \text{ m}^3$, thus ranking the eruption at VEI 3. The duration of the event was 17–18 days (see Section 2), and thus the mean discharge rate was on the order of $12 \pm 4 \times 10^3 \text{ kg/s}$. Using mass magnitude and intensity indexes of Pyle (2000), we obtain $M \sim 2.7$ and $I \sim 6.5$ when calculations are limited to the ash fall layer, but integration of the ballistic products yields $M \sim 3.2$ and $I \sim 7.0$. An error propagation analysis points to an uncertainty on the order of 0.3 on both M and I .

5.2. The late 1999 phase

The paucity of thickness data for the late 1999 phase hampered determining the VEI and mass magnitude of the activity, but many monitoring data allow us to compare with the August 2001 phase. Seismic recording by the IG-EPN in Quito identified 1756 explosions in the 28 Oct.–10 Dec. 1999 interval, i.e. an elevated average of ~40 explosions/day. Similarly, Cospec-based SO₂ output rates pointed to relatively high values in the range of 4–10 kt/day in the same period. The 75 satellite images revealed a fluctuating column height typically between ~6 and 12 km asl., but peaking at ~18 km asl on Dec. 6. In the collection, 91% of the images show a volcanic plume at relatively high elevations (>7.6 km asl), therefore injecting ash into mid-tropospheric air layers. The calculated average height of 9.3 km asl (i.e. 4.3 km above the crater) characterizes an elevated level of activity typical of *M*-type events in the present eruptive episode.

5.3. Weather conditions

The analysis of rain fall data for November and December in the 1983–2008 period yields a mean monthly precipitation of $71.8 \pm$

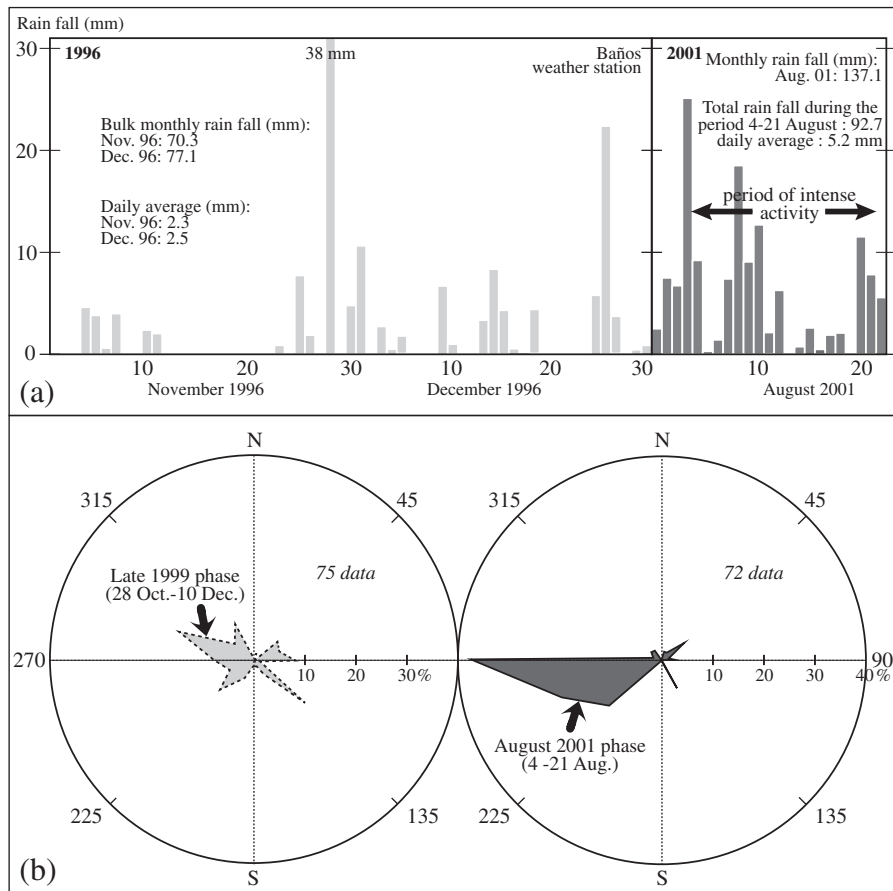


Fig. 6. Meteorological data selected to document seasonal weather conditions at Tungurahua volcano. (a) Rain fall data from Baños station illustrating a typical summer season in Nov.–Dec. 1996 (on the left), and a winter precipitation regime during the intense eruptive phase of August 2001 (on the right). (b) Rose diagrams wind distribution patterns at the plume altitude for periods of intense activity in late 1999 (left) and August 2001 (right).

37.5 mm/month, and a mean daily precipitation of 2.4 ± 1.2 mm/day, pointing out the relatively stable and dry weather conditions in Nov.–Dec. since 1983 in the Tungurahua area. These averaged values hide strong rain fall unsteadiness at shorter timescales, with series of dry days alternating with short-lived tropical rain storms (Fig. 6a left). These heavy rains are locally known as “aguaceros” (deluges), which typically produce lahars on the slopes of Tungurahua volcano since 1999. Our own observations in 1999 and comparisons with other weather data west of Tungurahua support a very similar precipitation regime for the Nov.–Dec. 1999 period. Rain during the 4–21 August 2001 interval displayed a different pattern (Fig. 6a right), with 92.7 mm recorded in 18 days, a daily rain height in the range of 0–25.0 mm/day, with a mean of 5.2 mm/day. At Tungurahua, such precipitation regime with low–moderate intensity rain falls is described as “Ilovizna” (drizzle or sprinkle) and sometimes produces modest muddy water flows on the volcano, but no lahars.

Although the wind flow distribution above Tungurahua shows fairly stable pattern at the multiyear scale (e.g. Fig. 4b of Arellano et al., 2008), significant differences occur between the Nov.–Dec. 1999 and the

August 2001 periods. The rose diagram of the late 1999 phase displays unsteady directions (Fig. 6b left), dominantly to the NW–SW, but also the E, NE and SE. Consistently, the volcanic clouds delineated on NOAA–VAAC satellite images show a widespread distribution (Fig. 7a). Low plumes are restricted to central Ecuador around Ambato and Riobamba cities, while higher plumes are dispersed in central and northern Ecuador, and also in southern Colombia and above the Pacific Ocean, north of Manta city (Fig. 7a). In contrast, the wind distribution pattern of the 4–21 August 2001 interval exhibits strong preferential flows to the W–SW (Fig. 6b right), and the envelope of ash clouds distribution exhibits a preferential dispersion to the W, mainly between Manta and Guayaquil cities for plumes below 7.6 km asl (Fig. 7b).

Overall, these weather results illustrate the seasonality in the Tungurahua region: the local “summer” season, which usually spans from October to February, consists of relatively hot and dry conditions with variable wind directions at crater altitude and above, while the “winter” season from late February to late September witnesses rather cold and rainy conditions, as well as dominant westward wind directions.

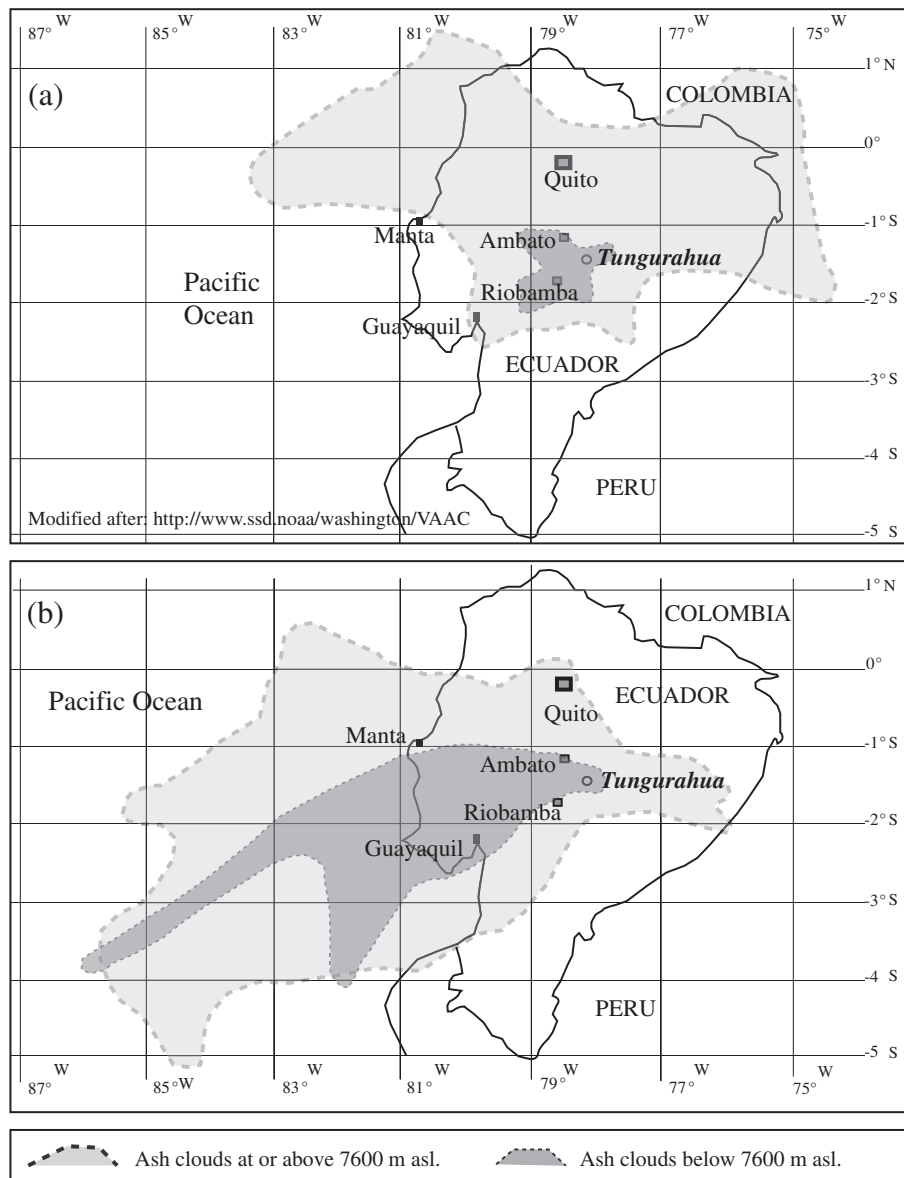


Fig. 7. Maps of the dispersal envelopes of volcanic ash clouds for the periods (a) Nov.–Dec. 1999 and (b) June–Sept. 2001, inferred from the inspection of NOAA–VAAC online archives. Dark gray areas are ash clouds detected below 7600 m, while light gray areas are ash clouds above 7600 m asl. Modified from Ruiz et al., 2004.

6. Discussion

6.1. Tephra thinning rate and volume

The complex segmentation of the August 2001 thickness decay rate suggests the intervention a several transport–depositional processes. The abrupt break-in-slope in the T vs. d plot (Fig. 3a) around 1.5 cm likely coincides with a change in dominant particle settling behavior, an issue that is beyond the scope of this note. The modest “secondary thickening” observed at $A^{1/2} \sim 7\text{--}8$ km (Fig. 5c) is probably not an artifact produced by uncertainties on thickness or isopach area data, but its origin remains unclear to us. Some ash aggregates were present in the deposits, as evidenced by a scanning electron microscopy study, but their abundance was too low to explain this bulge in the curve. Inspection of the relationship between topography and tephra layer thickness, and observations made in the course of the August 2001 phase suggest the importance of local near-ground winds on tephra redistribution at low elevation above the depositional area. The main plume was usually transported at $\sim 7\text{--}8$ km asl under westward wind flow (Figs. 3b and 7b). However, near-ground wind directions around Tungurahua are altered by topographic irregularities and differ from those at mid and high tropospheric levels; winds blowing from the Amazon lowlands run from East to West upward the Pastaza River valley, but rotate to the NW in the Patate River valley, and to the SW and S in the Chambo River valley (Fig. 1). The depositional area beneath the main plume axis coincided with two major topographic irregularities with a >1 -km deep V-shaped Guilles Ravine, and a wider U-shaped valley on the eastern flank of Iqualata volcano (Figs. 1 and 3). We surmise that these reliefs may have played a role on near-ground wind flows, resulting in local redistribution of volcanic ash during the eruption. If this interpretation is correct, the bulge should be interpreted as a secondary “over-thickening” anomaly, and nearby “holes” in the curve should correspond to an “under-thickening” due to ash remobilization. This mechanism is therefore different from other over-thickening processes such as ash aggregates accumulation in the layer (Carey and Sigurdsson, 1982; Brazier et al., 1983), local rain flushing and anticipated hydrometeor-enhanced particle deposition (Walker, 1981; Durant and Rose, 2009a, 2009b) or synchronous deposition of plume-derived tephra with elutriated co-pyroclastic flow ash (e.g. Eychenne et al., 2012).

6.2. Sizes of the 1999 and 2001 phases

This study raises questions on the relevance of ranking modern eruptions with a stepwise scale that is more appropriate to describe

ancient volcanic events (Newhall and Self, 1982; Siebert et al., 2011) and highlights the importance of near-vent coarse-grained ejecta on eruption size determination. Nevertheless, we surmise that the geological record of the August 2001 phase would rank the event at VEI 2, if estimated by current ground-based techniques. This is thus a small event when compared to other eruptions of the recent (<3 ka BP) geological history of the volcano (Hall et al., 1999; Le Pennec et al., 2006, 2008), and to the disastrous *L*-type August 2006 phase, whose tephra fall volume is estimated at $\sim 40\text{--}50 \times 10^6 \text{ m}^3$ (Eychenne et al., 2012). In terms of volume, the andesitic August 2001 Tungurahua ash layer is comparable to the 2001 scoria fall deposit from Etna (Scollo et al., 2007), and to older violent Strombolian to Subplinian eruptions from Vesuvius during the post AD 1631 activity (Arrighi et al., 2001). The intensity range is similar to that inferred for the 1975 eruption of Ngauruhoe volcano in New Zealand (Nairn and Self, 1978), the 1973 eruption of Heimaey in Iceland (Self et al., 1974), the 1995 Cerro Negro event in Nicaragua (Hill et al., 1998), the 1974 event of Fuego in Guatemala (Rose et al., 2008).

Available monitoring data suggest that the late 1999 phase was globally larger than the August 2001 phase, as evidenced by longer duration (6 vs. 2.5 weeks), higher explosion frequency (daily average of 40 vs. 7.5) higher mean plume elevation (9.3 vs. 8.4 km asl) and higher SO_2 output rate (4–10 kt/day vs. <4 kt/day). Yet, we consider that the late 1999 event as a whole was smaller than the powerful *L*-type event of August 16, 2006 ($M \sim 3.6$; Eychenne et al., work in progress). Therefore, the mass magnitude of the late 1999 phase was likely between 3.2 and 3.6.

6.3. Cause of major ash fall impact in August 2001

The eruptive conditions inferred for the August 2001 phase are representative of a typical *M*-type event at Tungurahua. By comparison with other *L*-type and *S*-type phases, these results suggest that eruptive intensities below $I \sim 6\text{--}7$ should result in inoffensive *S*-type eruptive phases, while intensities above $I \sim 7\text{--}8$ may lead to sustained tephra columns with generation of hazardous pyroclastic flows, as in July and August 2006, February 2008, May and December 2010. Monitoring short-term tephra output rate is therefore an important task for surveillance purpose at open-system volcanoes, as alert levels for potentially damaging ash falls and pyroclastic density current formation are partly grounded on these values.

Several factors may explain the different impacts of the 1999 and 2001 phases (Fig. 8). Sporadic storms in late 1999 rapidly eliminated most of the very thin ash layers. In addition, wind distribution results

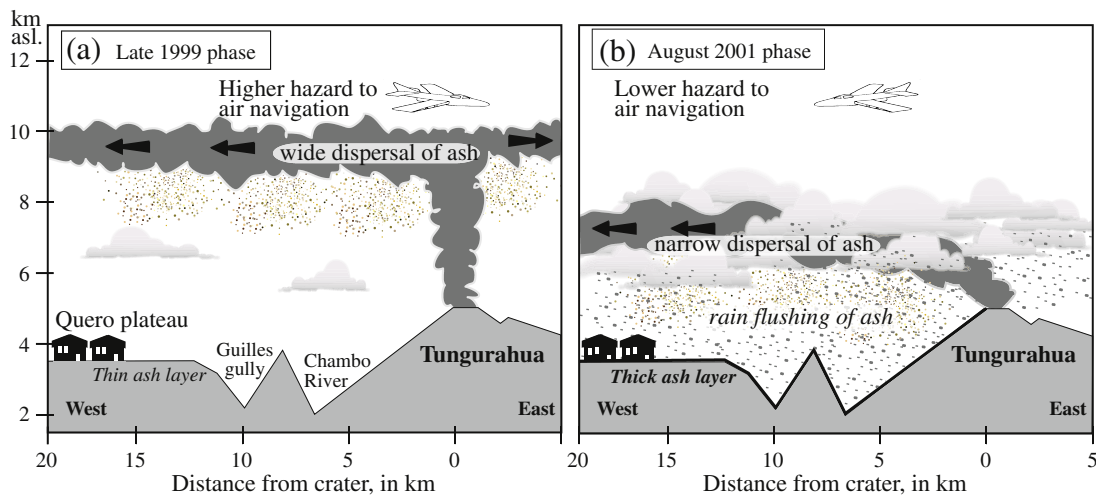


Fig. 8. Two cartoons depicting dissimilar ash dispersal patterns during (a) late 1999 and (b) August 2001 phases. (a) The dissemination of ash from a strong plume at high elevation during the dry summer season led to limited ash fall impacts in the vicinity of Tungurahua. (b) The sedimentation of ash from a bent-over plume inside a narrow region in the rainy winter season resulted in severe effects upon downwind rural and urban communities.

and satellite images (Figs. 6b and 7a) indicate that ash clouds during the relatively dry season in 1999 have been widely disseminated at high elevation (Fig. 8a), while near-ground winds which blown during many sunny afternoons removed most of the dry ash from roofs and leaves, resulting in limited impact on human health, buildings and farming. In summary, the impact was modest and did not reach the gravity witnessed in 2001.

In contrast, the August 2001 phase occurred in the rainy winter season (Fig. 8b), with a wind flow pattern that translated into a narrow depositional sector. Plume dispersion of the bent-over column occurred at lower elevation and mixed with rain clouds (Figs. 7b and 8b). Some diurnal wind shift effects from SW in the morning to NW in the afternoon have been observed, and this may partly explain the bilobate shape of the isopach contours in the Quero plateau (Fig. 3b). Similar wind-shifts and isopach shapes have been documented at other volcanoes (e.g. Cerro Negro in Nicaragua; Rose et al., 1973). In 2001, hygrometeors entrainment of the ash resulted in anticipated settling onto the ground at the scale of the whole depositional area. This process was apparent during the eruption through ash nuclei included as single or multiple grains in many rain droplets observed after their impact. Under dry weather conditions, as in late 1999, these particles would have been transported away beyond the Quero plateau (Fig. 1). Unlike the sporadic rain falls of the late 1999 period, the intensity of the August 2001 precipitations was usually too low to remove the ash cover, and the moist ash was compacted upon roofs and crops, forming a cohesive damaging coating.

7. Conclusion

Our assessment of the size of the August 2001 eruptive phase of Tungurahua volcano, Ecuador, indicates that it ranked near the limit VEI 2–3 or at VEI 3 when the ballistic tephra volume is considered. Mass magnitude (M) and intensity (I) indexes reach $M \approx 2.7$ and $I \approx 6.5$ when based solely on ash fall layer data, but increase to $M \approx 3.2$ and $I \approx 7.0$ when ballistic products are included. These results will allow us to calibrate the size of other eruptive phases in the course of the 1999-ongoing eruptive episode. Monitoring data suggest that the late 1999 phase was larger than the August 2001 phase, but the latter had a more harmful impact on Andean communities leaving west of the edifice. Our work indicates that the severe ash fall impact in August 2001 compared to that of 1999 is due to a subtle combination of unfavorable factors which included slightly different eruptive conditions and opposite seasonal regimes.

These findings highlight the importance of incorporating weather data in volcano alert messages to rural and urban communities in the tropical Andes. At Tungurahua, we show that a moderate-sized M -type eruptive phase in the winter season can rapidly turn into serious crises for nearby populations. Conversely, a larger long-lived phase in the dry season may have limited impact, although it can pose higher hazard to air navigation (e.g. Dec. 2010). These outcomes apply to many volcanic centers around the globe, notably in tropical and temperate countries.

Acknowledgments

This work has been carried out in the context of a cooperation program between the French Institut de Recherche pour le Développement (IRD) and the Instituto Geofísico of Quito's National Polytechnic School (IG-EPN), Ecuador. Financial support from both institutions is acknowledged. Many discussions with institutional representatives and testimonies offered by individuals in the Tungurahua area greatly helped us to improve our understanding of the 1999–2001 activity and impact. Journal reviews by R. Cioni and an anonymous Referee and editorial handling by L. Wilson helped to improve this paper. This is Laboratory of Excellence ClerVolc contribution no. 15.

References

- Almeida, E., Ramón, P., 1991. Las erupciones históricas del volcán Tungurahua. *Bol. Geol. Ecuat.* 2, 89–138.
- Arellano, S., Hall, M.L., Samaniego, P., Ruiz, A., Le Pennec, J.L., Molina, I., Palacios, P., Yepes, H., 2008. Degassing patterns of Tungurahua (Ecuador), during the 1999–2006 eruptive period, inferred from spectroscopic remote measurements of SO₂ emissions. *J. Volcanol. Geotherm. Res.* 176, 151–162. doi:10.1016/j.jvolgeores.2008.07.007.
- Arrighi, S., Principe, C., Rosi, M., 2001. Violent strombolian and subplinian eruptions at Vesuvius during post-1631 activity. *Bull. Volcanol.* 63, 126–150.
- Beddington, M., Cronin, S.J., Chapman, I., Turner, M.B., 2008. Quantifying volcanic ash fall hazard to electricity infrastructure. *J. Volcanol. Geotherm. Res.* 177, 1055–1062. doi:10.1016/j.jvolgeores.2008.07.023.
- BGVN, 1999–2010. Bulletin of the Global Volcanism Network, Monthly Reports (Period 1999–2010). <http://www.volcano.si.edu/world/volcano.cfm?vnum=1502-08=&volpage=var>.
- Bonadonna, C., Houghton, B.F., 2005. Total grain-size distribution and volume of tephra-fall deposits. *Bull. Volcanol.* 67, 441–456.
- Bonadonna, C., Ernst, G.G.J., Sparks, R.S.J., 1998. Thickness variations and volume estimate of tephra fall deposits: the importance of particle Reynolds number. *J. Volcanol. Geotherm. Res.* 81, 173–187.
- Brazier, S., Sparks, R.S.J., Carey, S.N., Sigurdsson, H., Westgate, J.A., 1983. Bimodal grain size distribution and secondary thickening in air-fall ash layers. *Nature* 301, 115–119.
- Carey, S.N., Sigurdsson, H., 1982. Influence of particle aggregation on deposition of distal tephra from the May 18, 1980 eruption of Mt. St. Helens volcano. *J. Geophys. Res.* 87, 7061–7072.
- Casadevall, T.J., 2003. The 1989–1990 eruption of Redoubt Volcano, Alaska: impacts on aircraft operations. *J. Volcanol. Geotherm. Res.* 62, 301–316.
- Connor, C.B., Hill, B.E., Winfrey, B., Franklin, N.M., La Femina, P.C., 2001. Estimation of volcanic hazards from tephra fallout. *Nat. Hazard Rev.* 2, 33–42.
- Cronin, S.J., Hedley, M.J., Neall, V.E., Smith, R.G., 1998. Agronomic impact of tephra fallout from the 1995 and 1996 Ruapehu Volcano eruptions, New Zealand. *Environ. Geol.* 34, 21–30.
- Durant, A.J., Rose, W.L., 2009a. Hydrometeor-enhanced tephra sedimentation: constraints from the 18 May 1980 eruption of Mount St. Helens (USA). *J. Geophys. Res.* 114, B03204.
- Durant, A.J., Rose, W.L., 2009b. Sedimentological constraints on hydrometeor-enhanced particle deposition: 1992 eruptions of Crater Peak, Alaska. *J. Volcanol. Geotherm. Res.* 186, 40–49.
- Eychenne, J., Le Pennec, J.L., Troncoso, L., Gouhier, M., Nedelec, J.M., 2012. Causes and consequences of bimodal grain size distribution of tephra fall deposited during the August 2006 Tungurahua eruption (Ecuador). *Bull. Volcanol.* 74, 187–205. doi:10.1007/s00445-011-0517-5.
- Fierstein, J., Nathenson, M., 1992. Another look at the calculation of fallout tephra volumes. *Bull. Volcanol.* 54, 156–167.
- Froggatt, P.C., 1982. Review of methods estimating rhyolitic tephra volumes; applications to the Taupo Volcanic Zone, New Zealand. *J. Volcanol. Geotherm. Res.* 14, 1–56.
- Hall, M.L., Robin, C., Beate, B., Mothes, P., Monzier, M., 1999. Tungurahua Volcano, Ecuador: structure, eruptive history and hazards. *J. Volcanol. Geotherm. Res.* 91, 1–21.
- Hall, M.L., Samaniego, P., Le Pennec, J.L., Johnson, J., 2008. Ecuadorian Andes volcanism: a review of Late Pliocene to Present activity. *J. Volcanol. Geotherm. Res.* 176, 1–6. doi:10.1016/j.jvolgeores.2008.06.012.
- Hill, B.E., Connor, C.B., Jarzempa, M.S., La Femina, P.C., Navarro, M., Strauch, W., 1998. 1995 eruptions of Cerro Negro volcano, Nicaragua and risk assessment for future eruptions. *Geol. Soc. Am. Bull.* 110, 1231–1241.
- Horwell, C.J., Baxter, P.J., 2006. The respiratory health hazards of volcanic ash: a review for volcanic risk mitigation. *Bull. Volcanol.* 69, 1–24.
- Houghton, B.F., Wilson, C.J.N., Pyle, D.M., 2000. Pyroclastic fall deposits. In: Sigurdsson, H., Houghton, B., Rymer, H., Stix, J., McNutt, S. (Eds.), *Encyclopedia of Volcanoes*. Academic Press, San Diego, pp. 555–570.
- Kelfoun, K., Samaniego, P., Palacios, P., Barba, D., 2009. Testing the suitability of frictional behaviour for pyroclastic flow simulation by comparison with a well-constrained eruption at Tungurahua volcano (Ecuador). *Bull. Volcanol.* 71, 1057–1075.
- Lane, L.R., Tobin, G.A., Witeford, L.M., 2003. Volcanic hazard or economic destitution: hard choices in Baños, Ecuador. *Environ. Hazard* 5, 23–34.
- Le Pennec, J.L., Ruiz, A.G., Mothes, P., Hall, M.L., Ramón, P., 2002. Maximum and minimum volume estimates of an ash-fall layer from the August 2001 eruption of Mt. Tungurahua (Ecuador). *V Internat. Symp. Andean Geodyn. (ISAG)*, Toulouse, France, *Extend. Abst.* pp. 371–374.
- Le Pennec, J.L., Ruiz, A.G., Mothes, P., Hall, M.L., Ramón, P., 2004. Estimaciones del volumen global del depósito de ceniza de la erupción de Agosto 2001 del volcán Tungurahua. *Bol. Invest. Geoci., 1. Instit. Geofís. Escuela Politéc. Nacional, Quito*, pp. 13–18.
- Le Pennec, J.L., Hall, M.L., Robin, C., Bartomioli, E., 2006. Tungurahua volcano – Late Holocene activity. *Field Guide A1. Fourth International Conference “Cities on Volcanoes”*, Quito, Ecuador. 24 pp.
- Le Pennec, J.L., Jaya, D., Samaniego, P., Ramón, P., Moreno, S., Egred, J., van der Plicht, J., 2008. The AD 1300–1700 eruptive periods at Tungurahua volcano, Ecuador, revealed by historical narratives, stratigraphy and radiocarbon dating. *J. Volcanol. Geotherm. Res.* 176, 70–81. doi:10.1016/j.jvolgeores.2008.05.019.
- Legros, F., 2000. Minimum volume of a tephra fallout deposit estimated from a single isopach. *J. Volcanol. Geotherm. Res.* 96, 25–32.

- McGimsey, R.G., Neal, C.A., Riley, C.M., 2002. Areal distribution, thickness, mass, volume, and grain size of tephra-fall deposits from the eruptions of Crater Peak vent, Mt. Spurr Volcano, Alaska. U.S. Geol. Surv. Open-File Rep. 370 pp.
- Molina, I.C., Kumagai, H., Le Pennec, J.L., Hall, M.L., 2005. Three-dimensional P-wave velocity structure of Tungurahua volcano, Ecuador. *J. Volcanol. Geotherm. Res.* 147, 144–156. doi:10.1016/j.jvolgeores.2005.03.011.
- Nairn, I.A., Self, S., 1978. Explosive eruptions and pyroclastic avalanches from Ngauruhoe in February 1975. *J. Volcanol. Geotherm. Res.* 3, 39–60.
- Newhall, C.G., Self, S., 1982. Volcanic Explosivity Index (VEI): an estimate of explosive magnitude for historical volcanism. *J. Geophys. Res.* 87, 1231–1238.
- OPS, 2000. Erupciones volcánicas y protección de la salud. Organization Panamerica de la Salud, Quito, Ecuador.
- Prata, A.J., 2009. Satellite detection of hazardous volcanic clouds and the risk to global air traffic. *Nat. Hazard* 51, 303–324.
- Pyle, D.M., 1989. The thickness, volume and grain-size of tephra fall deposits. *Bull. Volcanol.* 51, 1–15.
- Pyle, D.M., 1995. Assessment of the minimum volume of tephra fall deposits. *J. Volcanol. Geotherm. Res.* 69, 379–382.
- Pyle, D.M., 2000. Sizes of volcanic eruptions. In: Sigurdsson, H., Houghton, B., Rymer, H., Stix, J., McNutt, S. (Eds.), *Encyclopedia of Volcanoes*. Academic, San Diego, pp. 263–270.
- Rose, W.I., Bonis, S., Stoiber, R.E., Keller, M., Bickford, T., 1973. Studies of volcanic ash from two recent Central American eruptions. *Bull. Volcanol.* 37, 338–364.
- Rose, W., Self, S., Murrow, P., Bonadonna, C., Durant, A., Ernst, G., 2008. Nature and significance of small volume fall deposits at composite volcanoes: insights from the October 14, 1974 Fuego eruption, Guatemala. *Bull. Volcanol.* 70, 1043–1067.
- Ruiz, A.G., Barba, D.P., Yepes, H., Hall, M.L., 2004. Las nubes de ceniza del volcán Tungurahua entre Octubre 1999 y Septiembre 2001. *Invest. Geoci.* 1, 28–34.
- Ruiz, M., Lees, J.M., Johnson, J.B., 2005. Source constraints of Tungurahua explosion events. *Bull. Volcanol.* 68, 480–490. doi:10.1007/s00445-005-0023-8.
- Samaniño, P., Le Pennec, J.L., Robin, C., Hidalgo, S., 2011. Petrological analysis of the pre-eruptive magmatic process prior to the 2006 explosive eruptions at Tungurahua volcano (Ecuador). *J. Volcanol. Geotherm. Res.* 199, 69–84. doi:10.1016/j.jvolgeores.2010.10.010.
- Sarna-Wojcicki, A.M., Shipley, S., Waitt, J.R., Dzurisin, D., Wood, S.H., 1981. Areal distribution thickness, mass, volume, and grain-size of airfall ash from the six major eruptions of 1980. In: Lipman, W.P., Mullineaux, D.R. (Eds.), *Eruptions of Mount St. Helens*, Washington: U.S. Geol. Surv. Prof. Pap., 1250, pp. 577–600. Washington D.C.
- Scollo, S., Del Carlo, P., Coltelli, M., 2007. Tephra fallout of 2001 Etna flank eruption: analysis of the deposit and plume dispersion. *J. Volcanol. Geotherm. Res.* 160, 147–164.
- Scott, W.E., McGimsey, R.G., 1994. Character, mass, distribution, and origin of tephra-fall deposits of the 1989–1990 eruption of Redoubt volcano, south-central Alaska. *J. Volcanol. Geotherm. Res.* 62, 251–272.
- Self, S., Sparks, R.S.J., Booth, B., Walker, G.P.L., 1974. The 1973 Heimaey Strombolian scoria deposit, Iceland. *Geol. Mag.* 3, 539–548.
- Siebert, L., Simkin, T., Kimberly, P., 2011. *Volcanoes of the World*, Third Edition. University of California Press. 568 pp.
- Stewart, C., Johnston, D.M., Leonard, G.S., Horwell, C.J., Thordarson, T., Cronin, S.J., 2006. Contamination of water supplies by volcanic ashfall: a literature review and simple impact modeling. *J. Volcanol. Geotherm. Res.* 158, 296–306.
- Sulpizio, R., 2005. Three empirical methods for the calculation of distal volume of tephra-fall deposits. *J. Volcanol. Geotherm. Res.* 23, 39–68. doi:10.1016/j.jvolgeores.2005.03.001.
- Tobin, G.A., Whiteford, L.M., 2002. Community resilience and volcano hazard: the eruption of Tungurahua and evacuation of the Faldas in Ecuador. *Disasters: J. Disaster Stud. Policy Manag.* 26, 28–48.
- Tobin, G.A., Whiteford, L.M., 2004. Chronic hazards: health impacts associated with ongoing ash-falls around Mt. Tungurahua in Ecuador. In: Montz, B.E., Tobin, G.A. (Eds.), *Pap. Appl. Geogr. Conf.*, 27, pp. 84–93.
- Walker, G.P.L., 1981. Characteristics of two phreatoplinian ashes, and their water-flushed origin. *J. Volcanol. Geotherm. Res.* 9, 395–407.